Fatigue Performance and Microstructure of Pt-20Ir Wire and Its Coil For Medical Device Application

Bernard Li, Haitao Zhang and Kailynn Cho

Medtronic Neuromodulation
7000 Central Avenue NE, Minneapolis, MN 55432, US

Abstract. *Due to its good biocompatibility and its high corrosion resistance, Platinum and its alloys have been widely used in implantable medical devices, including neurovascular devices, cardiac rhythm management devices and neurological devices. Implantable neurostimulators have provided therapies to patients with chronic pain, movement disorders, and overactive bladder symptoms. For these therapies, well-controlled stimulation current is delivered to the target nerves through implantable leads. The implantable leads must have sufficient fatigue durability to last for many years of implantation. Although coils made with Pt-20Ir wire have been widely used in conductor leads from major medical device companies, its fatigue performance and microstructure has not been well studied. In this study, a newly developed axial fatigue test method was used to study the fatigue behavior of Pt-20Ir coil, and the fatigue behavior of the corresponding Pt-20Ir wire was studied using a rotary beam fatigue testing method. The fracture surfaces of Pt-20Ir wires and fractured coil filars were analyzed in SEM and compared. The slanted fracture surface was observed for Pt-20Ir coils, indicating that the axial fatigue of Pt-20Ir is multiaxial in nature. Multiaxial fatigue theory should be used to analyze coil axial fatigue behavior. The microstructure of Pt-20Ir cold worked wire for coil was also studied. The detailed microstructure such as crystallography texture and grain structures was analyzed by using SEM/EBSD method.*

INTRODUCTION

Implantable neurological devices are among the fastest-growing areas of the medical device industry. Implantable neurostimulators have provided therapy to patients with chronic pain [1-3], movement disorders [4-6], and overactive bladder symptoms [7-9]. For these therapies, well-controlled stimulation current is delivered to the target nerves through implantable leads. The implantable leads must have sufficient fatigue durability to last for many years of implantation. Platinum and its alloys have been applied in medical devices due to its stable chemical properties, its biocompatibility, its mechanical properties and its high charge density [10, 11]. It has been widely used in the electrodes of conductor leads from major medical device companies [12-14]. The Pt-20Ir wire has been used in lead conductors within the most sensitive human tissues, such as the thalamus in the brain, to stimulate the nerves. Deep Brain Stimulation (DBS) is one example that uses Pt-Ir wire as its lead conductors. Figure 1 shows an

implantable neurostimulator and its lead in the human body. The lead delivers an electrical signal from the implanted neurostimulator to the globus pallidus in the deep brain. As shown in Fig.1, the location of the leads may cause cyclic movement in the leads, which may result in certain fatigue damage on conductor wire. For lead design, in order to reduce the stress, lead conductors are typically designed in a coil shape, and usually Pt-20Ir wire is used. The MP35N is not a typical candidate for DBS applications. In cardiac rhythm management devices, MP35N wire usually is applied. To increase strength and fatigue life, the Iridium as an alloying element was added for solid solution strengthening. The high percentage cold work is intentionally applied to the wire to increase its strength for better fatigue performance.

Figure 1. Illustration of deep brain stimulator and its lead.

Although Pt-Ir wire has been used in DBS leads for many years, very little data on the fatigue performance is found in the public literature. Another area which lacks information is the cold worked Pt-Ir wire microstructure such as grain size. This is mainly because of the noble nature of the Pt-Ir alloy, which makes it difficult to use conventional metallographic methods to etch the Pt alloys and expose the grain structure. In this work, rotary bending fatigue testing was conducted to assess the fatigue behavior of the cold drawn platinum alloy wire with 20%Ir (Pt-20Ir). The fatigue behavior of Pt-20Ir was compared with that of MP35N wires. A non-traditional analytical method was used to reveal the microstructures of Pt-20Ir wire.

MATERIALS

The representative tensile property of cold-drawn 0.102 mm Pt-20Ir wire is shown in table 1. The Pt-20Ir wire has a chemical composition of 80% Pt and 20% Ir (wt.%) and was cold drawn.

Table 1 tensile mechanical properties of cold drawn Pt-20Ir wire

UTS, MPa	YS, MPa	E, GPa	Elongation, %
1231	1178	230	2.2

TEST METHOD

The fatigue test of the Pt-20Ir wire was performed in a rotary beam fatigue tester, which is shown in Fig. 2. Testing was performed at a frequency of 60 Hz. A spin fatigue tester from Valley Instrumentation was used for the testing. The testing equipment has a motor-driven chuck and a support bushing.

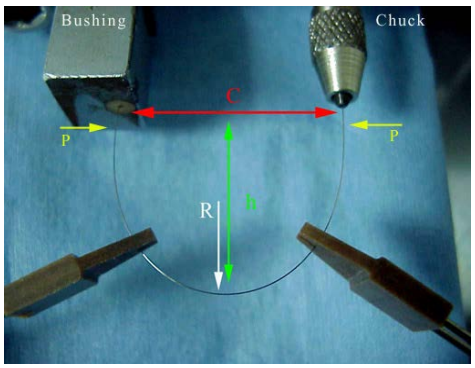

Figure 2. Wire rotary beam (spin fatigue) test setup.

During spin fatigue, the wire surface went through reversing cyclic strain. By using the conventional pure bending beam theory, the strain amplitude can be obtained by

$$\varepsilon = \frac{d}{2R} \qquad (1)$$

where d is the wire diameter and R is the bending radius of the wire. During testing, the support bushing can be adjusted to achieve the desired radius. The wire tensile properties were obtained with an Instron Universal Testing Machine with a 125N load cell. The test was displacement controlled. The loading speed was 76.2 mm/minute.

The Pt-20Ir wire was wound into a 4-filar coil with an outside diameter of 0.69 mm and coil pitch of 0.69 mm. The tension-tension test was performed on the coil. A Bose fatigue testing machine was used for the test. Each filar in the coil was electrically connected to detect the fatigue fracture during the test. The testing frequency is 30 Hz. The coil extension amplitude was calculated by using

$$\text{Extension amplitude} = \frac{L - L_0}{2L_0} \qquad (2)$$

The wire was mounted and final polished by using a vibratory polisher to remove the surface strain layer. Microstructure analysis of the sample was analyzed in longitudinal and transverse directions with a Zeiss Ultra scanning electron microscope (SEM) with electron backscattered diffraction (EBSD) imaging system (EDAX/OIM). The operation voltage was at 20kv.

RESULTS AND DISCUSSION

Wire Fatigue

Figure 3 is the strain life curve of Pt-20Ir wire from rotary bending test. The strain life curve of 0.102-mm diameter MP35N wire is also plotted to compare with Pt-20Ir wire. MP35N alloy is a Cobalt-based alloy with composition Co-35Ni-20Cr-10Mo which contains less than 1% Titanium. The fine MP35N wire is the most used lead conductor material in the medical device industry due to its mechanical properties, its fatigue performance and its physical properties. The MP35N wire is considered as a reference to other metal wires, though it is not a candidate for DBS applications. The strain life curve shows that the endurance limit strain of Pt-20Ir wire is about 0.18%, which is

about 45% of that of MP35N wire. The endurance limit is defined as the strain at 10^7 cycles. The LT MP35N is the low Titanium MP35N wire which shows an improved fatigue performance as compare to MP35N wire. The low Titanium MP35N contains Ti <0.01% in the alloy. Figure 4 is a fatigue fracture surface of Pt-20Ir wire after 5 million cycles at strain level 1.8%. The fatigue initiation is started from a surface defects (at 6 o'clock position). The crack propagation direction is perpendicular to the wire direction. The fracture surface is relatively flat which indicates the stress is in an

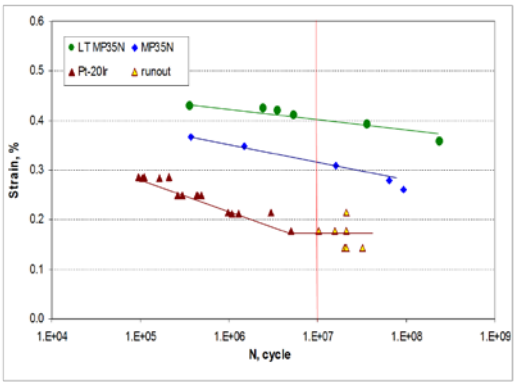

Figure 3. S-N (strain-life) curves of Pt-20Ir wire, MP35N and LT MP35N wires.

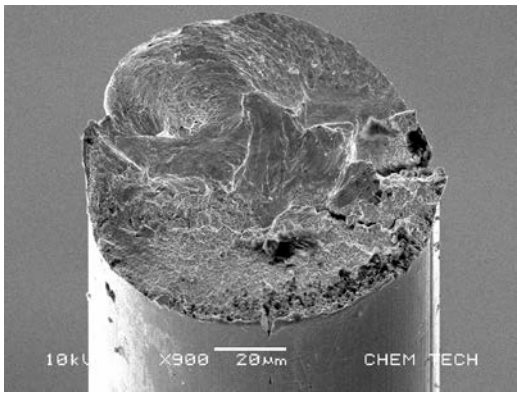

Figure 4. Fracture surface of a Pt-20Ir wire spin fatigue failed at $5x10^6$ cycles.

approximately uniaxial state. The fatigue crack propagation extended less than half of the wire diameter, after which it ruptured. The final fracture feature shows the torsion and ductile fracture.

Coil Tension-tension Fatigue

Axial fatigue tests were conducted at a frequency of 30 Hz with a BOSE fatigue tester. The lower fixture has an x-y stage to adjust the sample alignment. Each fixture has a cut-out slot to facilitate electric monitoring of the filar fracture. During testing, each filar was monitored individually. The testing sample has a gage length of 12.7 mm. The elongation selected are 11%, 12%, 13%, 15%, 16%, 17%, 18%, 19%, and 20%. The coil is mounted to the fixture through two lure fittings.

Figure 5 shows the fatigue Strain-Cycle Number (S-N) curve of the coil in extension amplitude versus life cycle. The fatigue endurance limit (FEL) difference between Pt-20Ir coil and MP35N coil is smaller than that of the wire spin fatigue data. As shown in table 2, the ratio of FEL Pt-20Ir wire to MP35N wire is 0.56. However, the ratio of FEL Pt-20Ir coil to MP35N coil is 0.89. The FEL of Pt-20Ir coil is closer to that of MP35N

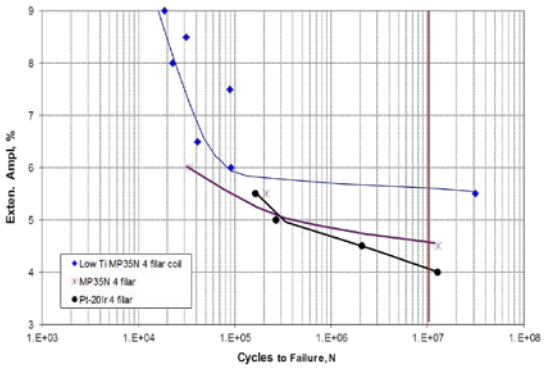

Figure 5 Coil tension-tension fatigue S-N curve (extension Amplitude- life cycle) of Pt-20Ir and MP35N coils.

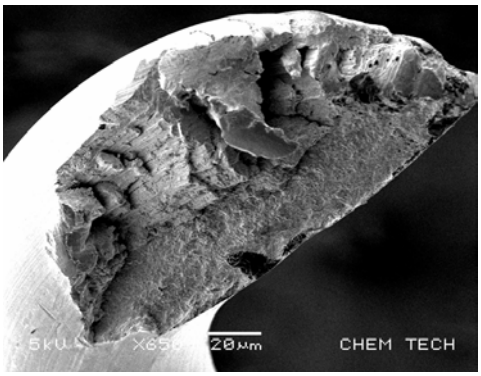

Figure 6 Fracture surface of a wire in coil failed at $2x10^6$ cycles. Multiaxial stresses cause fracture surface like a curved surface.

coil as compared to the wire. The difference between the two tests indicates the difference of stress states, resulting in fatigue performance of the wire. However, the FEL ratio between MP35N to LT MP35N is 0.8 in spin fatigue and 0.82 in coil tension-tension test. The ratio of FEL in these two tests is essentially the same, indicating that the Pt-20Ir wire fatigue performance is sensitive to the stress states. The multiaxial stresses in the coil results in a higher performance than that in single bending stress in wire spin fatigue. Figure 6 is a fracture surface from a wire of Pt-20Ir coil with 2.09 million cycles in tension. The fracture surface shows a significant different fracture plane to that of the wire fatigue fracture surface with respect to the wire direction. The coil fracture demonstrated multiple stresses occurred on the wire which forms a slanted fracture surface to the wire direction.

Table 2 Fatigue Endurance Limit (FEL) of Pt-20Ir Wire and Coil

Test Method	Unit	Pt-20Ir	MP35N	Ratio Pt-20Ir: MP35N	LT MP35N	Ratio MP35N: LTMP35N
Wire Spin fatigue	FEL, %	0.18	0.32	0.56	0.4	0.80
Coil tension-tension	FEL, %	4.0	4.5	0.89	5.5	0.82

Another major factor affecting the wire fatigue performance in the coil is the microstructure. The MP35N wire has an equiaxed grain structure and uniform texture through the wire diameter [15], however, Pt-20Ir wire has an elongated structure and a strong gradient from wire surface to wire core.

FEA Analysis of Coil Tension-tension Fatigue Sample

Before a filar fractures, filar-to-filar interaction is negligible. FEA stress and strain analysis can be conducted on a single filar. The length selected in the analysis is 5 revolutions. 11,616 linear hexahedral elements of type C3D8R were used. To assess the

surface stress accurately, 5,808 linear quadrilateral elements of type M3D4R with a thickness of 2.5 μm were "coated" on the surface of the quadrilateral elements. The coil

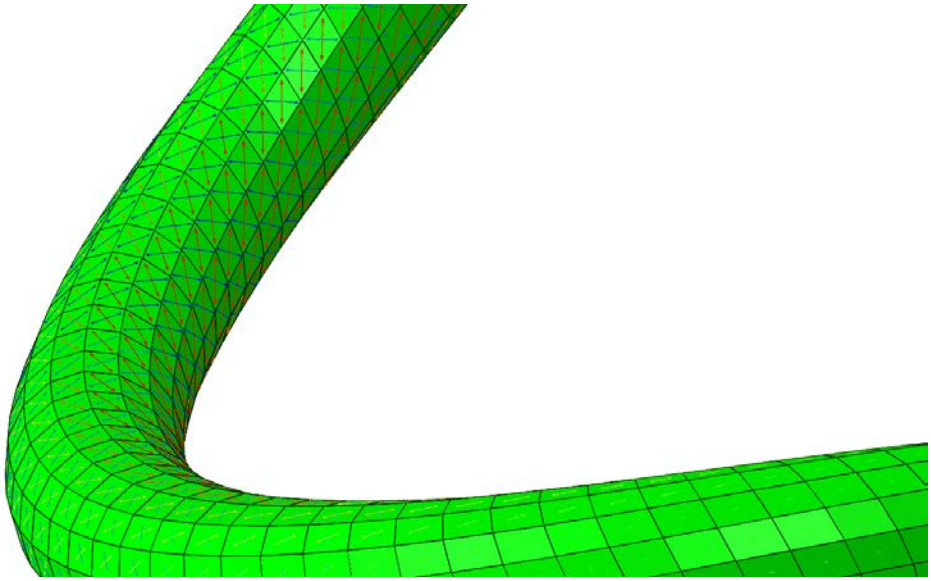

Figure 7 Maximum (red arrows) and minimum (blue arrows) principal strains on the coil surface.

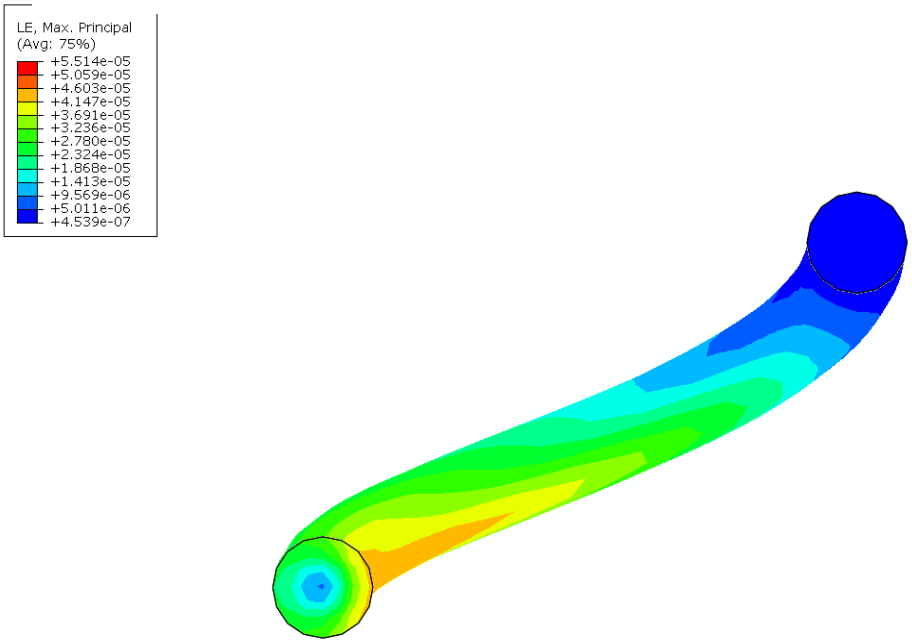

Figure 8 Maximum principal strains across the cross.

surface was in a multiaxial stress state. Figure 7 illustrates the maximum principal strain direction (tensile strain, in red arrows) and minimum principal strain (compression strain, in blue arrows). Figure 8 shows the maximum principal strain distribution on the cross section where the surface maximum principal strain has the largest value.

Microstructure of Pt-20Ir Wire

Due to the inert nature of Pt-20Ir alloy, it is very difficult to use conventional metallographic methods to reveal its grain structure. There is no etching agent able to etch the Pt-20Ir material since it is so chemically stable. To investigate the microstructure of the Pt-20Ir wire, a SEM/EBSD technique was used to investigate the grain structure of the Pt-20Ir wire. Figure 9 shows the grain orientation image of the Pt-20Ir wire in transverse direction; the color code shows the grain orientation of FCC structure, the triangle is the inverse pole figure of the cubic structure. The image in Figure 10 shows grain structure in longitudinal directions. The grain structure in the wire is elongated along the wire direction, indicating an unrecrystallized grain structure. The grain is in a cold drawn structure with a strong fiber textured structure.

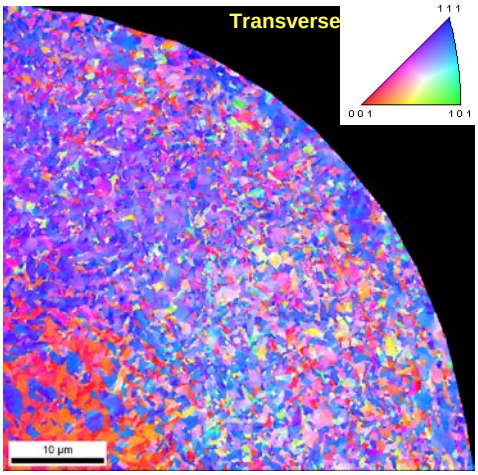

Figure 9. Grain orientation image of Pt-20Ir wire in transverse direction.

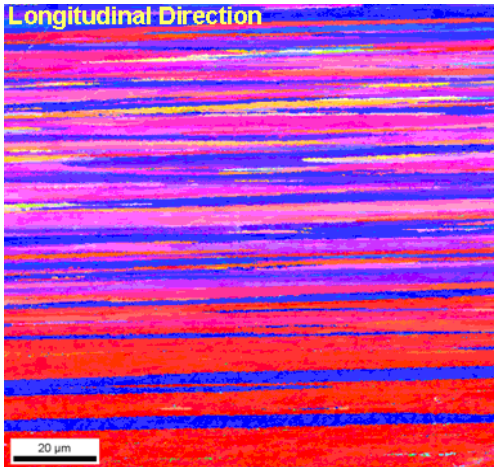

Figure 10. Grain orientation image of Pt-20Ir wire in longitudinal direction.

The images of Fig. 9 and Fig. 10 show texture gradients occurred in the Pt-20Ir wire, which are demonstrated by the color. In the center region, the area in red is highly <001> textured grain; the area near surface that is mostly blue is highly <111> textured grain; and the area in between the surface and the center is the transition area, which is mostly <113> textured grains. The grain structure shows highly deformed features of irregular shape (grains with pink and blue color). The highly deformed grain shows serrated grain boundaries in Figure 10 and 11a. Figure 11 shows the grain size map (a) and grain size distribution (b) in the transverse direction. The grain size map color matches the grain size distribution color. The grain size map shows that grains near the center of the Pt-20Ir wire have a larger size than those near the surface. The grain size distribution plot shows a lognormal distribution. The most likely grain size is between

0.25 and 0.3 μm. There is a long tail toward large grain size. Compared with cold drawn Pt-20Ir wire, the MP35N wire has a strong <111> textured grain, equiaxed grain structure and no strong texture gradients from wire center to surface [15]. The elongated

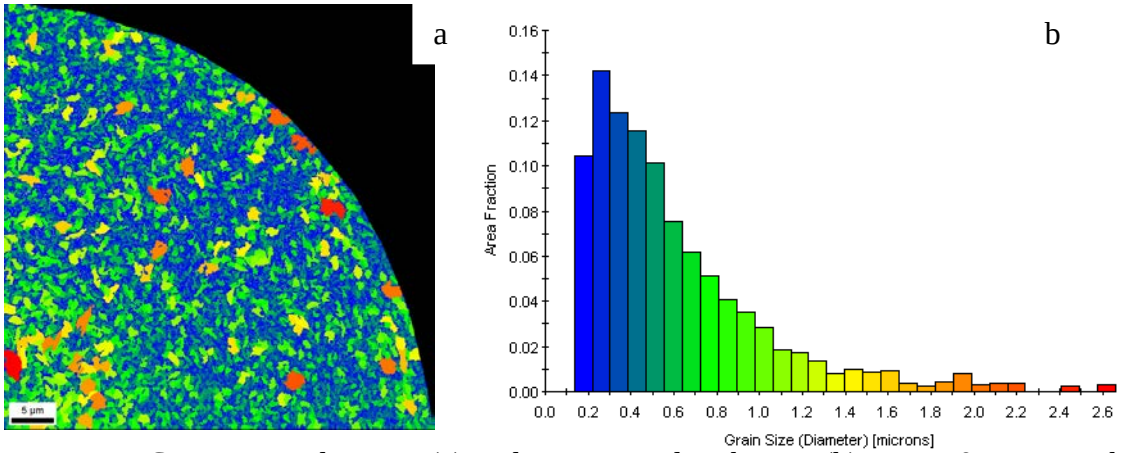

Figure 11. Grain size color map (a) and grain size distribution (b) in Pt-20Ir wire. The analysis area is in a transverse direction.

grain structure of Pt-20Ir wire indicates that the wire has unrecrystallized during the wire drawing process. The Pt-20Ir wire with fiber grain structure may have a different fracture feature under the cyclic multiaxial stress state such as torsion and tensile. The fiber grain structure delamination and crack propagation can occur along the wire direction, shown in the coil fatigue fracture surface. This changes the crack propagation directions and extendes the fatigue life.

CONCLUSION

Fatigue testing shows Pt-20Ir cold drawn wire (0.102 mm) has a fatigue endurance strain limit of 0.18%. Pt-20Ir Coil tension-tension fatigue data shows that the fatigue endurance limit (extension amplitude) is at 4.0%.

The elongated grain and multiaxial stresses are the key factors for Pt-20Ir coil tension-tension fatigue, close to that of MP35N coil. The microstructure of Pt-20Ir wire was characterized with SEM/EBSD technique. The grain size of the wire is elongated like a bundled fiber structure. The texture of wire is strongly fiber-textured and with a strong gradient from surface to center of the wire. Near-surface region has <111> textured grain and around center region of the wire has <100> textured grain. The center of grain also has a larger size than near surface.

REFERENCE

1. Barolat, G. and Sharan, A.D., 2004, "Spinal Cord Stimulation for Chronic Pain Management," Seminars in Neurosurgery, **15** (2/3), pp.151-175.

2. Cameron, T., 2004, "Safety and Efficacy of Spinal Cord Stimulation for the Treatment of Chronic Pain: a 20-year Literature Review," Journal of Neurosurgery: Spine, **100** (3 Suppl Spine), pp. 254-267.
3. Manchikanti, A., Boswell, M.V., Datta, S., Fellows, B., Abdi, S., Vijay Singh, V., Benyamin, R.M., Falco, F.J.E., Helm, S., Hayek, S., and Smith, H.S., 2009, "Comprehensive Review of Therapeutic Interventions in Managing Chronic Spinal Pain," Pain Physician, **12** (4), pp. E123-98.
4. Blomstedt, P., Hariz, M.I., 2010, "Deep Brain Stimulation for Movement Disorders before DBS for Movement Disorders," Parkinsonism & Related Disorders, **16** (7), pp. 429-433.
5. Benabid, A. L, Chabardes, S., Torres, N., Piallat, B., Krack, P., Fraix, V., Pollak, P., 2009, "Review Functional Neurosurgery for Movement Disorders: a Historical Perspective," Progress in Brain Research, **175**, pp.379-391.
6. Pizzolato, G., Mandat, T., 2012, "Deep Brain Stimulation for Movement Disorders," Frontiers in Integrative Neuroscience," **6** (2), pp.1-5.
7. Kohli, N. and Patterson, D., 2009, "InterStim® Therapy: A Contemporary Approach to Overactive Bladder," Reviews in Obstetrics and Gynecology, **2** (1), pp. 18-27.
8. Brazzelli, M., Murray, A. and Fraser, C., 2006, "Efficacy and Safety of Sacral Nerve Stimulation for Urinary Urge Incontinence: A Systematic Review," The Journal of Urology, **175** (3), pp.835-841.
9. Sherman, N. D., Jamison, M. G., George D. Webster, G. D., Amundsen, C. L., 2005, "Sacral Neuromodulation for the Treatment of Refractory Urinary Urge Incontinence after Stress Incontinence Surgery," American Journal of Obstetrics & Gynecology, **193** (6), pp. 2083-2087.
[10. Agnew, W. F.,Yuen, T. G. H., McCreery, D. B. and Bullara, L. A., 1986, "Histopathologic Evaluation of Prolonged Intracortical Electrical Stimulation," Experimental Neurology, **92** (1), pp. 162-185.
11. Brummer S. B. and Turner, M. J., 1977, "Criteria for Selecting Electrodes for Electrical Stimulation: Theoretical and Practical Considerations," IEEE Trans. Biomed. Eng., **24** (5), 440
12. Acta Med. Scand., 1969, **186** (S502), pp. 10–13.
13. Walton, C., Gergely, S. and Economides, A. P. 1987, "Platinum Pacemaker Electrodes: Origins and Effects of the Electrode-Tissue Interface Impedance," Pacing and Clinical Electrophysiology, **10** (1), pp. 87-99.
14. Winkle, R. A., Bach, S. M. , Mead, R. H. , Gaudiani, V.A., Stinson, , E. B., Fain E. S., and Schmidt, P., 1988, "Comparison of Defibrillation Efficacy in Humans Using a New Catheter and Superior Vena Cava Spring-left Ventricular Patch Electrodes," J. Am. Coll., **11** (2), pp.365-370.
15. Li, B. Q. and Steigauf, T., 2008, "Texture and Anisotropy of MP35N Wire " *Ceramic Transactions*, v 201, p 627-635, 2008, Applications of Texture Analysis - A Collection of Papers Presented at the 15th International Conference on Textures of Materials, ICOTOM